Water/Ethanol Soluble p-Type Conjugated Polymers for the Use in Organic Photovoltaics

frontiers in Materials

ORIGINAL RESEARCH
published: 14 August 2020
doi: 10.3389/fmats.2020.00281

Water/Ethanol Soluble p-Type Conjugated Polymers for the Use in Organic Photovoltaics

*Xun Pan[1], Anirudh Sharma[2], Renee Kroon[3], Desta Gedefaw[4], Sait Elmas[1], Yanting Yin[1], Gunther G. Andersson[1], David A. Lewis[1] and Mats R. Andersson[1]**

[1] Flinders Institute for NanoScale Science and Technology, Flinders University, Bedford Park, SA, Australia, [2] King Abdullah University of Science and Technology (KAUST), Physical Sciences and Engineering Division (PSE), KAUST Solar Center (KSC), Thuwal, Saudi Arabia, [3] Department of Chemical and Biological Engineering, Chalmers University of Technology, Goteborg, Sweden, [4] School of Biological and Chemical Sciences, The University of South Pacific, Suva, Fiji

We have developed two series of p-type conjugated polymers based on poly[2,3-bis-(3-octyloxyphenyl)quinoxaline-5,8-diyl-alt-thiophene-2,5-diyl] (TQ1) polymeric backbone utilizing polar pendant groups, i.e., tertiary amine and pyridine, to achieve switchable solubility in water and ethanol. By balancing the ratio between polar and non-polar side-groups, we could combine green-solvent processability with the manufacturing of functional photovoltaic devices. Due to the unavailability of water/alcohol soluble acceptors, the photovoltaic performance of these new polymers was evaluated using organic solvent by incorporating $PC_{61}BM$. For water/alcohol soluble partial amine-based polymers, we achieve a maximum power conversion efficiency (PCE) of ∼0.8% whereas alcohol soluble partial pyridine-based polymers show enhanced PCE of ∼1.3% with inverted device structure. We propose that the enhancement in PCE is a result of the reduction in amino-group content and the lower basicity of pyridine, both of which decrease the interaction between functionalized polymers with the anode interface material and reduce the miscibility of the donor and acceptor. Further improvement of the photovoltaic performance, in particular the open-circuit voltage (V_{OC}), was achieved by using an anode buffer layer to mitigate the unfavorable interaction of the amino/pyridine groups with the MoO_3 electrode. Our work demonstrated the possibility of substituent modification for conjugated polymers using tertiary amine and pyridine groups to achieve water/alcohol soluble and functional donor materials.

Keywords: side-chain modification, water/ethanol soluble, switchable solubility, conjugated polymers, organic photovoltaics

OPEN ACCESS

Edited by:
Erika Kozma,
Istituto per lo Studio delle Macromolecole (ISMAC), Italy

Reviewed by:
Chao Gao,
Xi'an Modern Chemistry Research Institute, China
Chunhui Duan,
South China University of Technology, China

****Correspondence:***
Mats R. Andersson
mats.andersson@flinders.edu.au

Specialty section:
This article was submitted to Energy Materials, a section of the journal Frontiers in Materials

Received: *29 May 2020*
Accepted: *27 July 2020*
Published: *14 August 2020*

Citation:
Pan X, Sharma A, Kroon R, Gedefaw D, Elmas S, Yin Y, Andersson GG, Lewis DA and Andersson MR (2020) Water/Ethanol Soluble p-Type Conjugated Polymers for the Use in Organic Photovoltaics. Front. Mater. 7:281. doi: 10.3389/fmats.2020.00281

INTRODUCTION

Over the past few years, a growing demand for green solvent processable conjugated materials has been witnessed in the field of organic photovoltaic (OPV) research (Xie et al., 2018; Xue et al., 2018; Lee S. et al., 2019) in order to realize the mass production of OPVs using low-cost and high-throughput printing method without the negative environmental effect caused by harmful halogenated solvent (Søndergaard et al., 2012; Angmo et al., 2013; Lee J. et al., 2019). Although

tremendous efforts have been put into the molecular design of conjugated polymers to push up the power conversion efficiencies (PCE) of single junction OPVs up to 18% (Liu et al., 2020), harmful, halogenated solvents such as chloroform, chlorobenzene or ortho-dichlorobenzene (*o*-DCB) are still widely used to dissolve the high-performing active materials for processing (Wang et al., 2017; Li X. et al., 2019; Fan et al., 2020). Using the materials that can only be processed with harmful solvents is undesirable for large-scale printing of OPVs due to the large quantities of solar ink required (Krebs et al., 2009, 2010), and diverges from the environmentally friendly aim of OPV (Søndergaard et al., 2011; Park et al., 2015). Recent research activities have studied more environmentally benign solvents such as anisole (Venkatesan et al., 2014), *o*-xylene (Xu et al., 2017; Yu et al., 2017), 2-methyl-tetrahydrofuran (Me-THF) (Fan et al., 2017; Li et al., 2018) and cyclopentyl methyl ether (Li Z. et al., 2019) for OPV manufacturing, achieving comparable or even better device performance to the OPVs fabricated using halogenated solvents. However, these non-halogenated solvents still pose a health-risk to the ecosystem and are cost-ineffective due to their high price and the necessary solvent recovery system.

Using water or ethanol as basis for solar inks is an ideal solution to fulfill the aim of green and low-cost processing of OPVs. One solution is offered through water dispersed nanoparticles (NPs) based on conjugated materials to realize the fabrication of OPVs from the most ideal eco-friendly solvent, water. The use of NP inks additionally circumvents the tedious development of water-soluble semiconducting donor and acceptor pairs with high PCE (Gärtner et al., 2014; Holmes et al., 2016; D'Olieslaeger et al., 2017; Almyahi et al., 2018; Pan et al., 2018). The fabrication process of NP-inks is, however, not without issues, as the NP preparation via miniemulsion method is a time-consuming process and requires both insulating surfactants and chlorinated precursor solvents (Colberts et al., 2017) while most of NPs made by precipitation method (Schwarz et al., 2015) suffer from high instability of the final solar ink (Geoffrey et al., 2018).

In another approach, water/alcohol soluble conjugated polymers (WS) have been investigated as active layer materials for water/alcohol-based solar inks. Through the side-chain engineering (Huang et al., 2010; Mei and Bao, 2013; He et al., 2014; Hu et al., 2015; Park et al., 2015; Wu et al., 2016) i.e., replacing the hydrophobic aliphatic substituent with hydrophilic polar side groups, for example, ionic moieties [e.g., sulfonate groups (Mwaura et al., 2005), quaternary ammonium salt (Hu et al., 2015)] and non-ionic functional groups such as tertiary amine (Duan et al., 2013; Li et al., 2013; Lv et al., 2014; Ma et al., 2014; Cai et al., 2015) and oligoethylene glycol (OEG) (Søndergaard et al., 2011; Nguyen et al., 2017; Kim et al., 2018; Lee et al., 2018). However, the ionic moieties have been reported to act as charge carrier traps/recombination site (Yang et al., 2007; Duan et al., 2013), and the WSCPs designed based on this approach have only been successfully applied as interface layer materials for OPVs (Huang et al., 2010; Wu et al., 2016; Xu B. et al., 2016). OPVs based on active layer fabricated from WSCP elaborated with tertiary amine functionalities showed no photovoltaic response (Duan et al., 2013). So far, the highest photovoltaic performance was reported by Lee, S. et al., achieving 2.15% PCE with OEG-functionalized water/alcohol soluble active materials (Lee S. et al., 2019).

In this work, we have modified the polymer, poly[2,3-bis-(3-octyloxyphenyl)quinoxaline-5,8-diyl-alt-thiophene-2,5-diyl] (TQ1) (Wang et al., 2010; Sharma et al., 2017), by complete or partial replacement of the aliphatic solubilising side-chains with side groups having tertiary amine and pyridine groups. In this way, a series of new polymers were obtained that allowed us to study the effect of functional group loading on the solubility in water/alcohol. The new polymers have been evaluated in solar devices using classic PCBM to prove their efficacy as electron donors. Our results show that switchable water/ethanol soluble p-type conjugated polymers can be achieved and using pyridine pendant groups can give decent photovoltaic performance, which will be beneficial for environmentally friendly fabrication of OPVs in the future.

EXPERIMENTAL

All reactions were performed under nitrogen protection unless otherwise stated. Chemicals were commercially available from Sigma-Aldrich and used without further purification. 5,8-Dibromo-2,3-bis(3-(octyloxy)phenyl)quinoxaline and 2,5-bis(trimethylstannyl)thiophene were purchased from Solarmer Energy, Inc., and the latter was purified by recrystallisation from methanol. All solvents were used as obtained from supplier except toluene, which was dried and distilled prior to the polymerisation reactions. Experimental procedures are available in the electronic **supplementary information** (ESI). The structures of the synthesized small molecular compounds were confirmed by ^{1}H-NMR spectra measured on Bruker 300 MHz NMR spectrometer. The ^{1}H-NMR spectra of all polymers were measured on Bruker 600 MHz NMR spectrometer. The recorded ^{1}H-NMR were referred to tetramethylsilane (TMS) as internal standard.

Material Characterization

Gel-permeation chromatography (GPC) measurements were performed at 35°C on an Agilent PL-GPC 220 equipped with a differential refractive index detector. Dimethylformamide (DMF) was used as eluent at a flow rate of 1.0 mL/min, and the solvent DMF as well as sample solutions were filtered through a filter with the pore size of 0.45 μm (Nylon, Millex-HN 13 mm Syringes Filters, Millipore, United States). The number average molecular weights (M_n) and polydispersity index (PDI) were calculated using a calibration curve based on polyethylene glycol (PEG) standards.

The ultraviolet–visible (UV–vis) study was performed on a Perkin Elmer UV–vis-NIR Lambda950 spectrophotometer.

Thermogravimetric analysis (TGA) measurements were performed on TA instruments Discovery TGA series TGA1-0288, with the temperature range of 25 –400°C under nitrogen gas flow, and the heating ramp of 10°C/min. The acid treated polymer samples were prepared by dissolving polymer in ethanol with 3% formic acid prior to drop casting on freshly cleaned

glass substrate, followed by drying in air and then collected with a scalpel. Prior to the TGA measurements, the collected solid samples were further dried overnight in a vacuum oven at room temperature. The isothermal process was conducted in the TGA under a nitrogen gas flow of 25 mL/min.

Cyclic voltammetry (CV) measurements were performed using a 0.1 M solution of tetrabutylammonium hexafluorophosphate (Bu_4NPF_6) in anhydrous acetonitrile as the supporting electrolyte and a Ag/Ag^+ quasi reference electrode. The ferrocene/ferrocenium (Fc/Fc^+) reference was used to calibrate the measurements. The highest occupied molecular orbital energy levels (E_{HOMO}) and the lowest unoccupied molecular orbital energy levels (E_{LUMO}) were estimated from the onset potentials by setting the oxidative potential of Fc/Fc^+ vs the normal hydrogen electrode (NHE) to 0.630 V, and the NHE vs the vacuum level to 4.5 V (Hellström et al., 2009; Gedefaw et al., 2017b).

Device Fabrication

Inverted solar cells with the structure ITO/ZnO/bulk-heterojunction (BHJ)/MoO_3/Ag or ITO/ZnO/BHJ/N,N′-bis(3-methylphenyl)-N,N′-bis(phenyl)-benzidine (TPD)/MoO_3/Ag were fabricated using fixed weight ratio of 1:2.5 donor-polymer:$PC_{61}BM$ in the active layer. Patterned ITO-coated glass substrates (10 Ω/sq, purchased from Xin Yan Technology Ltd.) were cleaned using the procedure published elsewhere (Sharma et al., 2017). ITO-coated glass substrates were cleaned by soaking in a 5% detergent solution (pyroneg from Johnson Diversey) at 90°C for 20 min and then rinsing in deionized (DI) water, before sonicating in DI water, acetone and isopropanol for 10 min each. Substrates were then cleaned in UV–ozone for 20 min immediately before spin coating the ZnO layer. ZnO sol–gel (Sun et al., 2011) on the cleaned ITO substrate was thermally annealed at 280°C for 10 min in air to yield a 25–30 nm thick film. The BHJ layers were spin-coated in the glove box to give approximate 80 nm thickness. In the case of TPD being introduced in the device, a TPD buffer layer (3 nm) was thermally evaporated on top of the BHJ layer (using a Covap system supplied by Angstrom Engineering) before depositing 12 nm of MoO_3 hole transport layer (using a Covap system supplied by Angstrom Engineering). Finally, the Ag electrode (80 nm) was deposited by thermal evaporation through a shadow mask, which defined the active area to be 0.1 cm^2.

Device Characterization

Photovoltaic properties of solar cells were measured in air by an Oriel solar simulator fitted with a 150 W xenon lamp (Newport), filtered to give an irradiation of 100 mW/cm^2 at an atmospheric mass (AM) of 1.5 and calibrated using a silicon reference cell with NIST traceable certification. The photocurrent–voltage (I–V) characteristics of the devices were measured through a Keithley 2400 source meter unit.

Atomic force microscopy (AFM) (supplied by Bruker, Billerica, MA, United States) was performed in tapping mode using silicon tips. The films were spin-coated from the same solutions used for device fabrication, on freshly cleaned ITO-coated glass substrates.

Electron Spectroscopy

Ultraviolet photoelectron spectroscopy (UPS) measurements were performed under an ultra-high vacuum (UHV) apparatus built by SPECS (Berlin, Germany) using a low intensity UV light source (HeI) with an excitation energy of 21.21 eV, to measure the work functions, as described elsewhere (Sharma et al., 2017). The UPS samples were prepared by thermally evaporating MoO_3 (12 nm) on freshly cleaned glass substrates in a vacuum deposition chamber followed by spin-coating polymer solution (1 mg/mL *o*-DCB) at 500 rpm for 60 s and 3000 rpm for 30 s in a glove box under nitrogen. The prepared samples were transferred from the glove box to the load lock for UPS measurements using a nitrogen filled zip-lock bag.

RESULTS AND DISCUSSION

Material Synthesis

The quinoxaline moieties were chosen as the site for modification of the pendent groups due to the relatively simple chemistry to attach a hydrophilic group (Gedefaw et al., 2017a). The structure and synthesis procedures are shown in **Scheme 1**.

The Williamson etherification between compound **1** and 3-dimethylamino-1-propylchloride hydrochloride led to compound **2** as yellow oil after purification via column chromatography. Although different parameters such as temperature, solvent and the purity of starting materials were explored to improve the reaction yield, the maximum yield was only about 14% conversion. Better yield was achieved in the synthesis of TQ1A monomer **4**. The monomer was prepared through condensation of compound **2** and **3** followed by purification via column chromatography and recrystallisation, and the pale yellow monomer **4** was obtained in 87.4% yield.

To prepare quinoxaline monomer with pyridine side groups, firstly compound **5** was synthesized from commercially available 4-pyridinepropanol by reacting with HBr under reflux overnight. It is worth noting that 4-(3-bromopropyl)pyridine was intrinsically unstable and protonation of the compound with HBr was necessary to be able to isolate the compound. The TQ1P4 monomer **7** was synthesized through Williamson etherification between compound **5** and compound **6** in refluxed acetonitrile (MeCN). The structures of the quinoxaline monomers with tertiary amine side groups and pyridine side groups were confirmed by ^{1}H-NMR spectroscopy (**Supplementary Figure S1**) and detailed synthetic procedures can be found in the **Supplementary Information**.

Polymer TQ1A was synthesized via Stille coupling by polymerizing monomer **4** and 2,5-bis(trimethylstannyl)thiophene using freshly distilled toluene as the solvent. A significant amount of precipitate was observed over the course of the reaction when using pure toluene to synthesis TQ1P4, hence, a more polar solvent blend of dry toluene/DMF (4:1 volume ratio) was used to increase the solubility of pyridine polymer during the polymerisation reaction. The copolymers TQ1-50A, TQ1-20A, TQ1-50P4, and TQ1-20P4 were polymerised using three monomers with different molar ratio to obtain the products with different loading

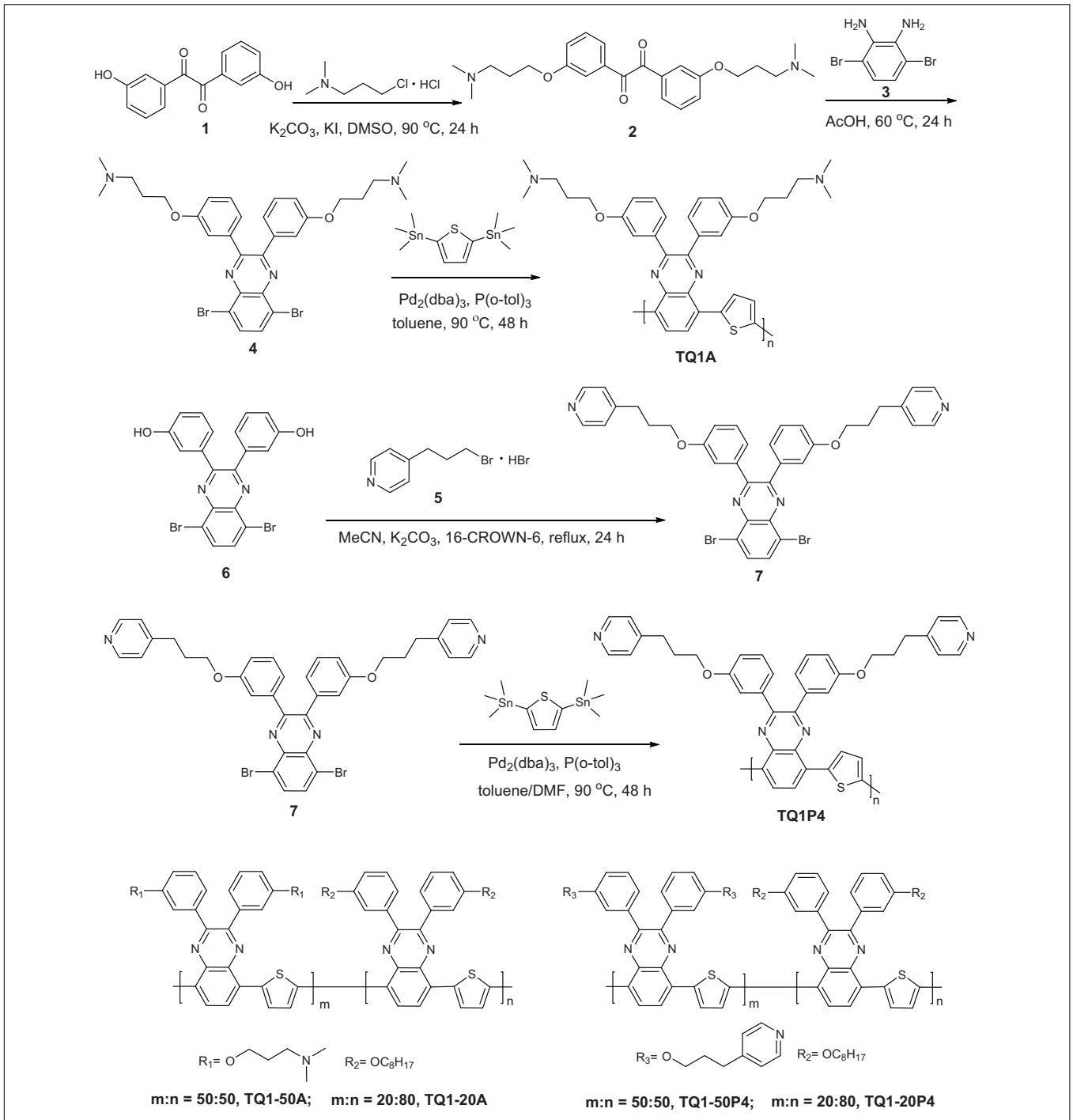

SCHEME 1 | Synthetic route for polymers with amino side groups and pyridine side groups.

of functional groups attached to the polymer backbone. The ratio between the functional polar groups and octyl groups in the polymers was confirmed by their ^{1}H-NMR spectra (see **Supplementary Figure S2** and **Supplementary Table S1**).

The number average molecular weights (M_n) of TQ1P4 and TQ1-50P4 were measured to be 9.6 and 8.6 kg/mol with the PDI of 2.7 and 4.3, respectively. The low M_n was likely a result from the limited solubility of oligomer/polymers in the toluene/DMF reaction solvent, which impeded the chain growth during the coupling reaction. The molecular weights of amino polymers and TQ1-20P4 could not be measured due to their limited solubility in DMF and tetrahydrofuran (THF). In addition, 1,2,4-trichlorobenzene (1,2,4-TCB) has also been tried as the eluent for GPC measurements of amine-functionalized

polymers, but no response was observed, which was probably caused by the adhesion of the amino groups to the columns and the metal tubing.

Optical Properties and Switchable Solubility in Green Solvents

We first probed the solubility of the synthesized polymers in ethanol and water acidified with formic acid (FA), to have an indication how their solubility depends on the concentration of functional groups. The amine-functionalized polymer TQ1A and TQ1-50A showed good solubility in water and ethanol with a small amount of FA (3% v/v), due to the protonation of tertiary amine forming conjugated polyelectrolyte. Similarly, attributing to the localization of the lone-pair electrons on the nitrogen atoms in sp^2 orbital, pyridine can also be easily protonated by FA to generate a pyridinium salt. Hence, TQ1P4 was found to be soluble in acidic water/ethanol in concentrations that are typical for solar cell inks, and TQ1-50P4, containing 50% pyridine in the quinoxaline unit, can be dissolved in ethanol (EtOH) with FA. The UV–vis spectra of these two new series of polymers in chloroform and green solvents were compared with the solid states, and the polymer solutions in water and ethanol are shown in **Figure 1**. The ethanol and water solution of TQ1A revealed a slightly enhanced absorption (**Figure 1A**), which can be a result from the ion introduced electrostatic perturbation (Wu et al., 2016). However, the TQ1-50A (**Figure 1B**) aqueous solution exhibits reduced absorption in the low-energy band while the

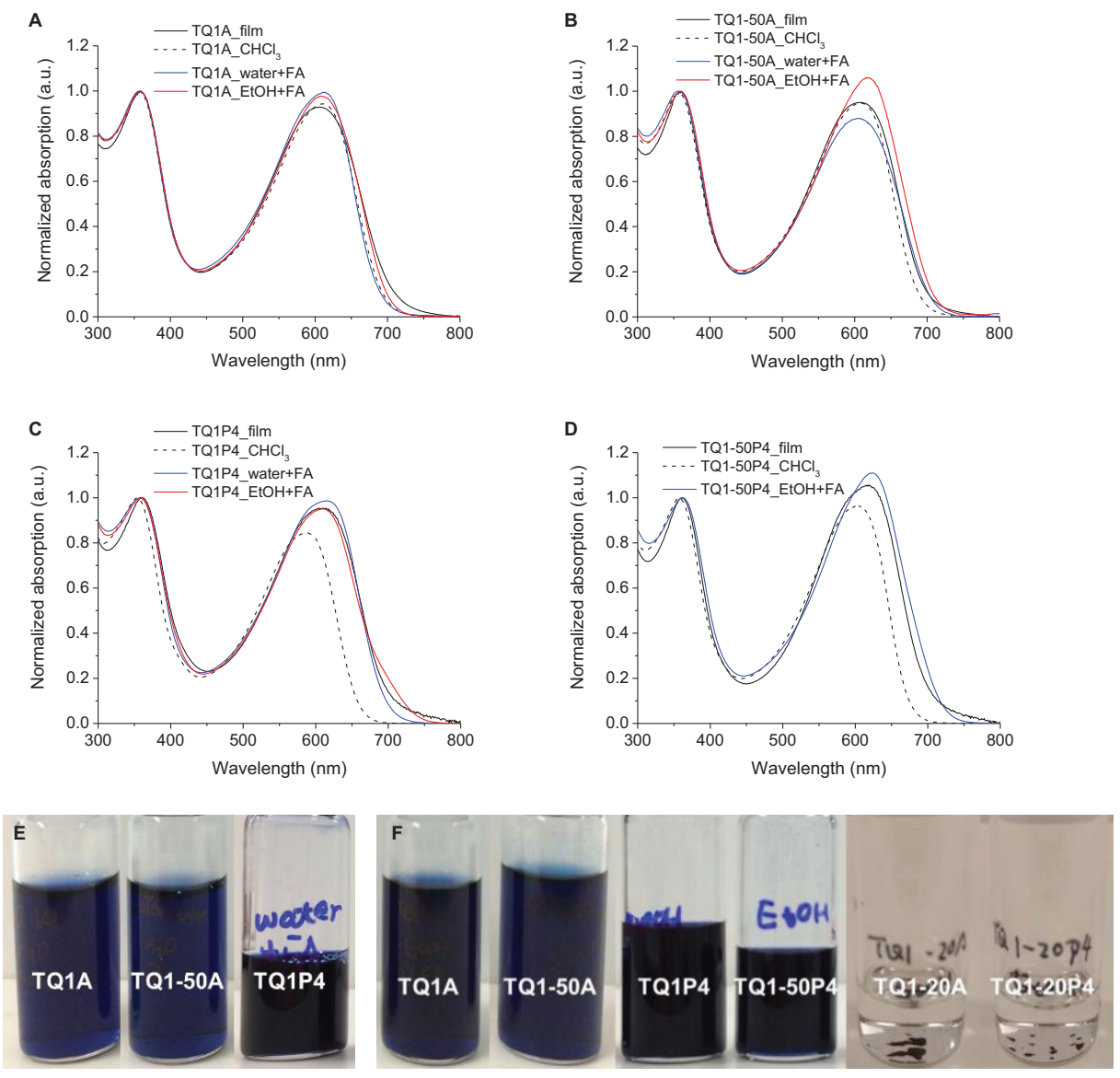

FIGURE 1 | Normalized UV–vis absorption spectra of **(A)** TQ1A, **(B)** TQ1-50A, **(C)** TQ1P4, and **(D)** TQ1-50P4 in different solvents and in the solid state. Photographs of **(E)** polymer in water + 3% FA solution, **(F)** polymer in EtOH + 3% FA solution.

opposite behavior is observed in ethanol solution, which could be explained by the influence of solvent on the charge transfer state or different degrees of torsion/planarity in polymer backbone using different solvents (Kroon et al., 2012).

The UV–vis absorption of the pyridine polymers in the solid states are virtually identical to the amino analogs. The absorption bands of TQ1P4 film (**Figure 1C**) were enhanced and red-shifted in the long wavelength region compared to the chloroform solution, which is presumably due to the higher intermolecular interaction and/or better packing in the solid condition. Red-shifted absorption spectra were also found in the aqueous and ethanol solutions of protonated polymer compared to the neutral polymer in chlorinated solvent, indicating multichain aggregation (Dang et al., 2016) or solvatochromic effects resulted from the polar solvent (Woo et al., 2005; Wu et al., 2016). Similar absorption behavior was also found in the UV–vis spectra of TQ1-50P4 (**Figure 1D**).

TQ1-20A and TQ1-20P4 could not be dissolved in EtOH + 3% FA (**Figure 1F**), presumably due to the low content of the tertiary amine or pyridine substituent in the conjugated polymer structure. The large number of octyl groups inhibits the switching of polymer solubility assisted by acid. The UV–vis spectra of TQ1-20A and TQ1-20P4 in chloroform solutions and in the solid state (**Supplementary Figure S3**) present similar absorption properties compared to TQ1A and TQ1P4, respectively.

Since ionic side groups presented in photoactive layers are known to be unfavorable for efficient charge transfer (Yang et al., 2007; Nguyen et al., 2017), it is important to study the possibility of regenerating neutral polymers after acidified water/ethanol processing.

TGA measurements were performed on protonated and unprotonated TQ1A and TQ1P4 (**Figure 2**), revealing FA release under heating, as significant weight losses from about 100 to 150°C were observed in the protonated samples. After holding the FA treated TQ1A isothermally at 120°C, the sample did not exhibit any further weight loss before the polymer degraded above 300°C (**Figure 2A**). Due to the weaker basicity of pyridine compared to tertiary amine, it was suspected that part of the binding acid had already released during the pre-drying of protonated TQ1P4 under vacuum, thus the weight loss of FA treated TQ1P4 is relatively lower than for the amino counterpart (**Figure 2B**). The TGA results reveal a mild thermal treatment of the protonated polymer in the solid state (120°C for TQ1A and 110°C for TQ1P4) could effectively remove FA and regenerate the neutral polymers. Furthermore, we found that the deprotonation procedure under isothermal process was completed in about 10 min for bulk material as shown in **Supplementary Figure S4**. Hence, it is possible to process functional polymers using green solvents in the presence of a volatile acid and achieve neutral polymer films in the fabrication of OPVs under mild condition. This highly reversible process is depicted in **Scheme 2**, showing the protonation and deprotonation process of pyridine-functionalized polymer TQ1P4. This switchable solubility observed in the new polymers could also be beneficial for various electronic applications (Hellström et al., 2011; Xing et al., 2018).

Electrochemical Properties

The electrochemical properties of new polymers presented in this work were investigated by cyclic voltammetry (CV). Compared to the reported TQ1 (Wang et al., 2010), tertiary amine or pyridine functionalized polymers in the solid states all exhibit near-identical optical bandgaps and similar energy levels (see **Supplementary Table S2** and **Supplementary Figure S5**), indicating that the modification of substituents attached to the quinoxaline backbone have a negligible influence on the conjugation of the resulting polymers.

It has been previously reported that amino groups are potential hole traps in the BHJ devices containing amine-functionalized active materials, due to that the highest occupied molecular orbital (HOMO) level of p-type polymer lies below the oxidation state of amine (Cai et al., 2015). Hence, electrochemistry was also performed on triethylamine to compare its oxidation process with amine-functionalized TQ1A. Furthermore, since we are the first to report pyridine substituted

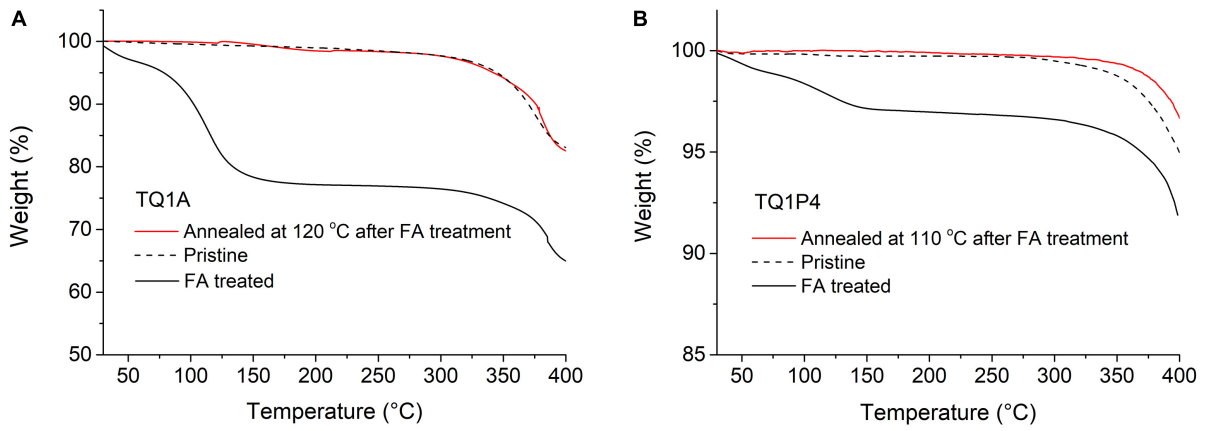

FIGURE 2 | TGA plots of **(A)** TQ1A sample treated with formic acid and then thermally annealed at 120°C for 10 min, with neat TQ1A and FA treated TQ1A as references and **(B)** TQ1P4 sample treated with formic acid and then thermally annealed at 110°C for 10 min, with neat TQ1P4 and FA treated TQ1P4 as references.

polymer as electron-donor in the BHJ system, the oxidation process of pyridine was carefully studied to compare with that of TQ1P4. The CV oxidation curves of amino compounds are presented in **Figure 3A**, showing an onset oxidation potential of TQ1A conjugated backbone to be 0.34 V vs Fc/Fc^+, which is similar to the onset oxidation potential of triethylamine (∼0.32 V). Thus, the HOMO of TQ1A lies very close or slightly below the ionization state of amine side groups. This result raised our concern about the viability and effectiveness of utilizing amine-functionalized p-type polymers in OPVs. Nevertheless, the onset oxidation potential of pyridine was measured to be ∼1.0 V, which is far above the value for the TQ1P4 backbone of 0.32 V (**Figure 3B**), revealing the low-lying ionization state of pyridine groups compared to the pyridine-functionalized polymer. Hence, the introduced side-chain with pyridine pendant group potentially affects hole transfer in the pyridine-functionalized polymer to a much lower degree compared to tertiary amine functionalities (Cai et al., 2015). The irreversibility of the CV is also a concern for the use of the materials in OPV devices, however, some high performing donor polymers used in OPVs also exhibit irreversible CVs (Xu X. et al., 2016; Zhang et al., 2017; Li et al., 2018).

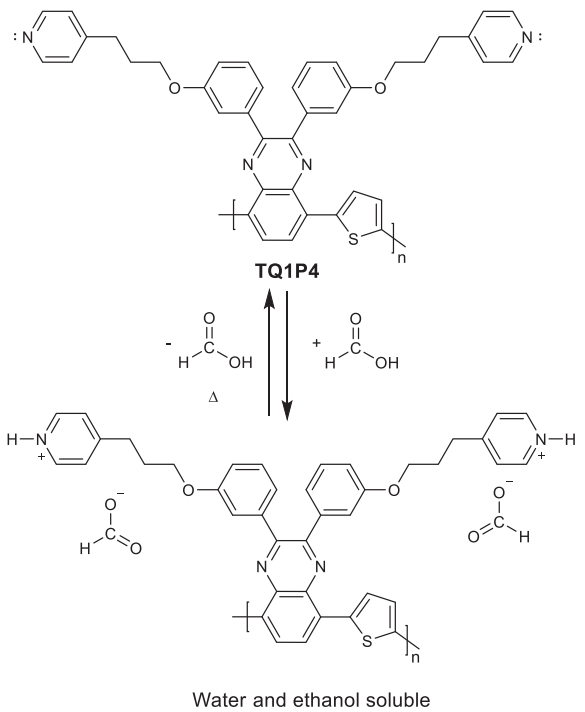

SCHEME 2 | Protonation of pyridine-functionalized polymer TQ1P4 using formic acid and the deprotonation process to remove formic acid under heating.

Interfacial Engineering

Materials with amino and pyridine functionalities have been previously reported as interface layers to reduce the electrode work function (Duan et al., 2013; Wu et al., 2016; Sharma et al., 2017), which is related to the presence of nitrogens with free electron pair in these materials. Since tertiary amines and pyridine groups are well known for reducing the work function of the underlying metal oxide electrodes (van Reenen et al., 2014; Cai et al., 2015; George et al., 2016), studying these donor polymers in devices with an inverted structure (ITO/ZnO/BHJ/MoO_3/Ag) would be ideal as the work function of the underlying cathode layer would be further altered in an energetically favorable direction. However, it is equally important to also understand the interaction of the amine/pyridine groups of the donor polymer with the top anode interface, due to its potential to influence the energetics at the BHJ-MoO_3 interface.

The water contact angle value of neat TQ1A and TQ1A:$PC_{61}BM$ blend films were found to be similar (**Supplementary Table S3**), indicating a high content of amino polymer on the top surface of the BHJ layer (toward the air interface) after spin-coating. The presence of amino groups toward the air interface makes the potential interaction between amines and MoO_3 layer highly likely in an actual device.

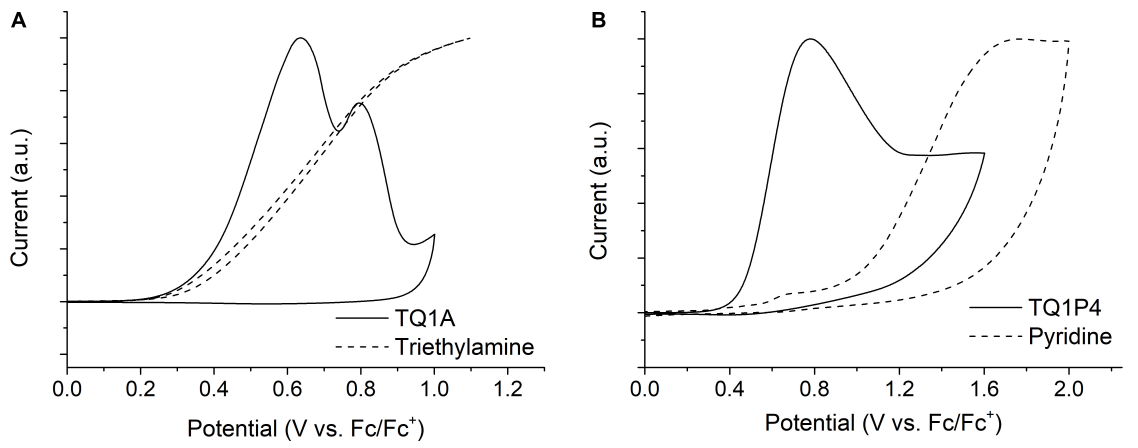

FIGURE 3 | Cyclic voltammetry (CV) oxidation curves of **(A)** TQ1A in the solid state and triethylamine in solution, **(B)** TQ1P4 in the solid state and pyridine in solution.

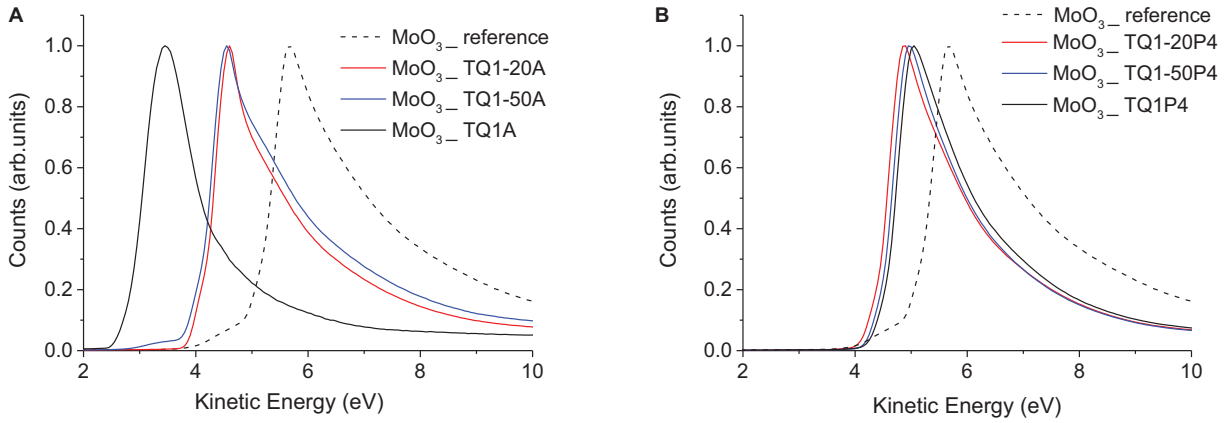

FIGURE 4 | UPS spectra of *o*-DCB washed MoO_3 reference and **(A)** thin layer of amino polymer coated MoO_3 samples, **(B)** thin layer of pyridine polymer coated MoO_3.

Therefore, to gain more insight into the work function modification of MoO_3 as a result of its interaction with the tertiary amine or pyridine groups in working devices, UPS measurements were performed on evaporated MoO_3 with a thin layer of spin-coated functional polymer on top. The work function of freshly evaporated pristine MoO_3 sample was found to be 5.4 eV (**Supplementary Figure S6**). Since the polymer films were deposited from *o*-DCB solution, the work function of MoO_3 washed with *o*-DCB was also measured to study any changes in the MoO_3 work function due to surface treatment with *o*-DCB. The work function of *o*-DCB treated MoO_3 was found to be slightly reduced to 5.3 eV and was used as a reference for MoO_3 in this study. The difference in the absolute work function value of MoO_3 measured in this study (5.4/5.3 eV) as compared to 6.7 eV reported in literature (Kröger et al., 2009; Meyer et al., 2012) can be attributed to slight air/humidity exposure during the sample transfer and mounting.

Modification of the MoO_3 surface with a thin layer of TQ1-50A and TQ1-20A was found to markedly reduce the work function of MoO_3 by around 1.0 eV, as seen by the shift in the secondary electron cut off from 5.3 to 4.3 eV (**Figure 4A**). Furthermore, the work function of MoO_3 was significantly shifted from 5.3 to 3.0 eV upon coating an extremely thin layer of TQ1A. While these results show the strong ability of amino polymers to alter the surface properties of transition metal oxides, it also opens up the possibility of selectively tuning their electronic functionalities, i.e., being switched from being an anode interface layer to a cathode interface layer. Our UPS findings showed significant change in the MoO_3 work function post modification with amino polymer and its possible utilization as a bi-functional interlayer was validated by the photovoltaic response measured from solar cells incorporating these interlayers (ITO/MoO_3/TQ1A/BHJ/MoO_3/Ag) (see **Supplementary Table S4**).

TQ1P4 and its analogs were also found to significantly reduce the work function of MoO_3 as seen from a shift of ∼0.7 eV in the secondary electron cut-off of the spectra (**Figure 4B**). However, the relatively smaller shift in the case of TQ1P4 as compared to TQ1A indicates that the interaction between pyridine and MoO_3 is weaker as compared to tertiary amine.

Photovoltaic Performance

To evaluate the photovoltaic properties of tertiary amine/pyridine-functionalized polymers in solar cell devices, a typical fullerene derivative, $PC_{61}BM$, was used as an acceptor due to the lack of a readily available water or ethanol soluble acceptor material in this study. Thus, we used *o*-DCB and anisole to process solar inks containing $PC_{61}BM$ for BHJ OPVs. Anisole, which has also been used in some recent studies (Venkatesan et al., 2014; Zhang et al., 2016), was selected as a relatively greener solvent of choice compared to its halogenated counterparts. In addition, anisole was utilized to process the TQ1P4 and TQ1-50P4 containing active layer due to the limited solubility of these two pyridine polymers in *o*-DCB, revealed from large polymer aggregations in *o*-DCB processed films (**Supplementary Figure S7**). However, the amino polymers and TQ1-20P4 could not be completely dissolved in anisole with the concentrations ideal for device fabrication, thus, *o*-DCB was chosen to process amino polymers and TQ1-20P4 containing active layer to offer better film quality for proper evaluation of their photovoltaic properties.

Devices based on TQ1A:$PC_{61}BM$ BHJ layer and an inverted structure (ITO/ZnO/BHJ/MoO_3/Ag) showed very limited PCE of 0.07%, with J_{SC} of 0.93 mA/cm^2 and V_{OC} of 0.18 V (**Table 1**). The significant voltage loss could be a result of the unwanted interaction between tertiary amine groups and MoO_3, or the complex formed between tertiary amine and $PC_{61}BM$, which could lead to severe charge recombination (Ghosh et al., 1993). To improve the device performance, the BHJ and the anode interface was carefully engineered by inserting an additional thin organic hole transport layer of N,N′-bis(3-methylphenyl)-N,N′-bis(phenyl)-benzidine (TPD) (Ishii et al., 1999; Lu et al., 2013) between the BHJ and the MoO_3. A thin layer of TPD was utilized to not only reduce the unwanted interaction between polar pendant groups and MoO_3 as seen from UPS studies, but it has previously been shown to enhance the blocking of electrons

TABLE 1 | Photovoltaic performance of the best BHJ OPVs based on TQ1A, TQ1-50A, TQ1-20A, TQ1P4, TQ1-50P4, and TQ1-20P4 with $PC_{61}BM$ (fixed Donor:Acceptor 1:2.5 weight ratio) blends with device structure of [a]ITO/ZnO/BHJ/TPD/MoO_3/Ag and [b]ITO/ZnO/BHJ/MoO_3/Ag.

Polymer	Device structure	BHJ solvent	J_{SC} (mA/cm^2)	FF (%)	V_{OC} (V)	PCE (%)
TQ1A	a	*o*-DCB	0.94	43	0.34	0.13
	b		0.93	39	0.18	0.07
TQ1-50A	a	*o*-DCB	4.17	43	0.46	0.82
	b		3.37	43	0.41	0.59
TQ1-20A	a	*o*-DCB	3.95	46	0.58	1.06
	b		3.94	46	0.54	0.97
TQ1P4	a	Anisole	2.19	43	0.60	0.57
	b		1.53	36	0.47	0.26
TQ1-50P4	a	Anisole	4.23	54	0.59	1.33
	b		5.07	43	0.51	1.11
TQ1-20P4	a	o-DCB	5.67	47	0.65	1.75
	b		5.79	47	0.62	1.69

at the anode interface (Subbiah et al., 2010; Lu et al., 2013). Upon applying a thin layer of TPD (3 nm), the V_{OC} was marginally improved to 0.34 V, leading to an efficiency of 0.13%. Although the devices based on TQ1A showed photovoltaic response, the PCE is much lower compared to that of TQ1:$PC_{61}BM$ devices (Kroon et al., 2012), which could be due to the charge traps formed by the amino groups, indicated from the electrochemistry results (Cai et al., 2015).

To further understand the OPV devices containing amine-functionalized donor polymer, polymers substituted with 50 and 20% amine groups were studied subsequently. For the optimized device structure with an additional TPD passivation layer, replacing TQ1A with TQ1-50A and TQ1-20A resulted in enhanced PCEs of 0.82 and 1.06%, respectively. While the J_{SC} was increased from 0.93 mA/cm^2 (TQ1A) to 4.17 mA/cm^2 (TQ1-50A), and 3.95 mA/cm^2 (TQ1-20A), the V_{OC} also saw an improvement from 0.34 V (TQ1A) to 0.46 V (TQ1-50A), and 0.58 V (TQ1-20A). These results show a strong dependence of the J_{SC} and V_{OC} on the tertiary amine content in donor polymers, in particular for devices without TPD. It is worth noting that with the decrease of amine content in the BHJ layer, the difference in the average photovoltaic performance with and without TPD becomes less significant (**Figure 5** and **Table 1**) and is consistent with the UPS results showing the interaction between the amine-functionalized polymer and MoO_3 became weaker with less tertiary amine loading.

Inverted devices having the structure ITO/ZnO/BHJ/MoO_3/Ag where the BHJ was composed of TQ1P4:$PC_{61}BM$ were found to have a maximum J_{SC} of 1.53 mA/cm^2, FF of 36%, and V_{OC} of 0.47 V, resulting in a PCE of 0.26%, which is notably higher compared to their TQ1A counterparts. The PCE was further improved to 0.57%, with an enhancement of FF to 43%, V_{OC} to 0.6 V and J_{SC} to 2.19 mA/cm^2, when an additional TPD layer was used. For optimized devices with the BHJ composed of TQ1-50P4:$PC_{61}BM$ and TQ1-20P4:$PC_{61}BM$, the PCEs were found to increase to 1.33% (J_{SC} = 4.23 mA/cm^2, FF of 54%) and 1.75% (J_{SC} = 5.67 mA/cm^2, V_{OC} of 0.65 V), respectively (**Figure 5** and **Table 1**). As seen in the case of the pyridine-functionalized polymers, the J_{SC} is increasing significantly with the decrease of pyridine content in the polymer structure (**Figure 5D**), while V_{OC} was found to be less dependent on the pyridine content (**Figure 5E**). The representative J–V plots are shown in **Supplementary Figure S9**.

While polymers substituted with 50 and 100% of tertiary amine and pyridine side groups show excellent solubility in ethanol with acid, the PCE of the pyridine-based polymer (TQ1-50P4) was found to be 62% higher than that for TQ1-50A. Thus, utilizing materials such as TQ1-50P4 for polymer solar cells may be a good compromise between the green solvent solubility and acceptable photo-conversion efficiencies.

Active Layer Morphology

The molecular weight of the amine/pyridine based TQ1 is relatively low compared to other conjugated systems. To determine the impact of molecular weight on performance, TQ1 with a comparably low molecular weight (LMW) (M_n = 10.8 kg/mol, PDI = 2.0) was synthesized and evaluated in BHJ devices incorporating $PC_{61}BM$ with the same device geometry (**Supplementary Table S5**). The maximum PCE of OPV based on LMW-TQ1:$PC_{61}BM$ was found to be 2.55% (J_{SC} = 5.77 mA/cm^2, V_{OC} = 0.85 V, and FF = 52%), which is comparably lower than the high molecular weight counterpart (Kroon et al., 2012). Hence, the low PCEs observed in amine/pyridine polymer based devices could be partly explained by the low molecular weight of our polymers. To further understand the lower photovoltaic performance of these functional polymers compared to their unfunctionalized counterpart TQ1, atomic force microscopy (AFM) was performed to investigate the surface topography of blend films with different donor polymers.

The AFM image of the TQ1A:$PC_{61}BM$ blend film (**Figure 6A**) reveals an extremely smooth surface with the root-mean-square roughness (R_q) value of only 0.5 nm, indicating a highly miscible morphology on the surface. The lack of phase separation between donor-rich phase and acceptor-rich phase can be a result from interaction between tertiary amine and the fullerene (Ghosh et al., 1993), which could lead to high degree of charge recombination. In the case of lower content of tertiary amine, an increase in R_q was observed as well as more phase separated feature being indicated (**Figures 6B,C**). To further probe the extent of miscibility between amine-functionalized polymer with $PC_{61}BM$, differential scanning calorimetry (DSC) was performed on amino polymer:$PC_{61}BM$ blends with different donor:acceptor (D:A) weight ratios and a TQ1:$PC_{61}BM$ blend as the reference, the DSC curves were taken from the second scan (see **Supplementary Figure S8**). We found that amino polymer was intimately mixed with $PC_{61}BM$ at respective D:A ratios based on the absence of a melting behavior for $PC_{61}BM$, suggesting the presence of a homogenous phase or new complex (Bernardo et al., 2016). We also found a clear trend that the miscibility between amino polymer and $PC_{61}BM$ decreased when the tertiary amine content in the polymers decreased, revealed from the detected melting

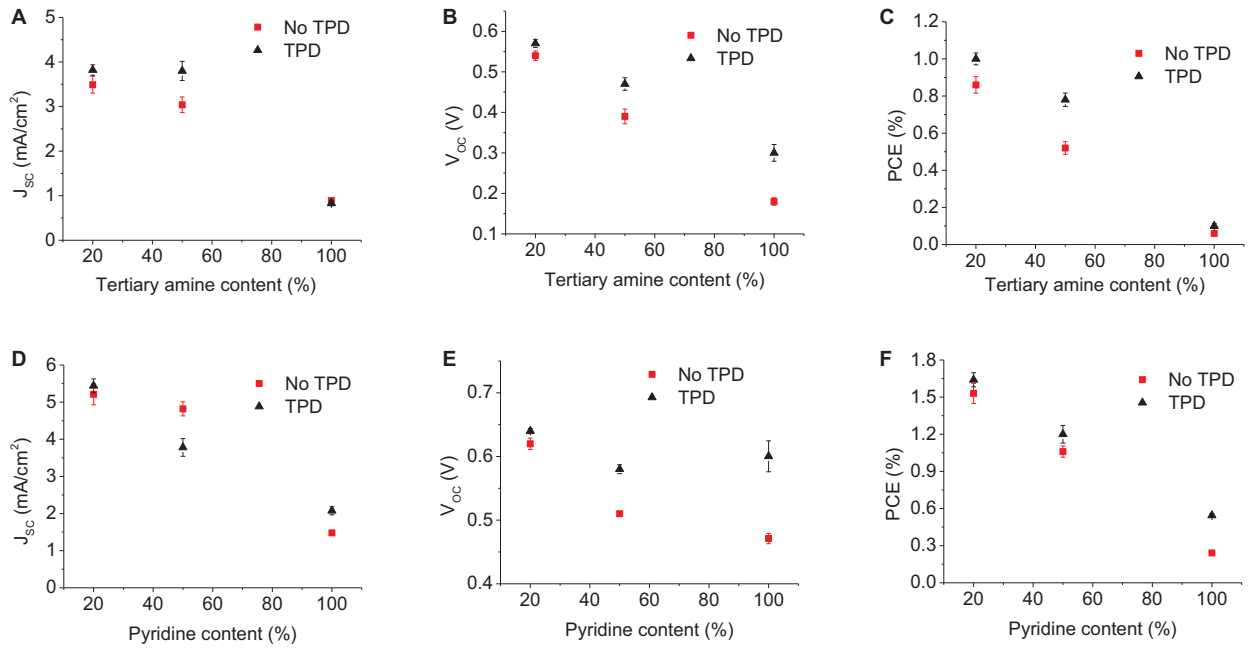

FIGURE 5 | Device characteristics as a function of tertiary amine **(A–C)** and pyridine content in the quinoxaline unit of polymers **(D–F)**.

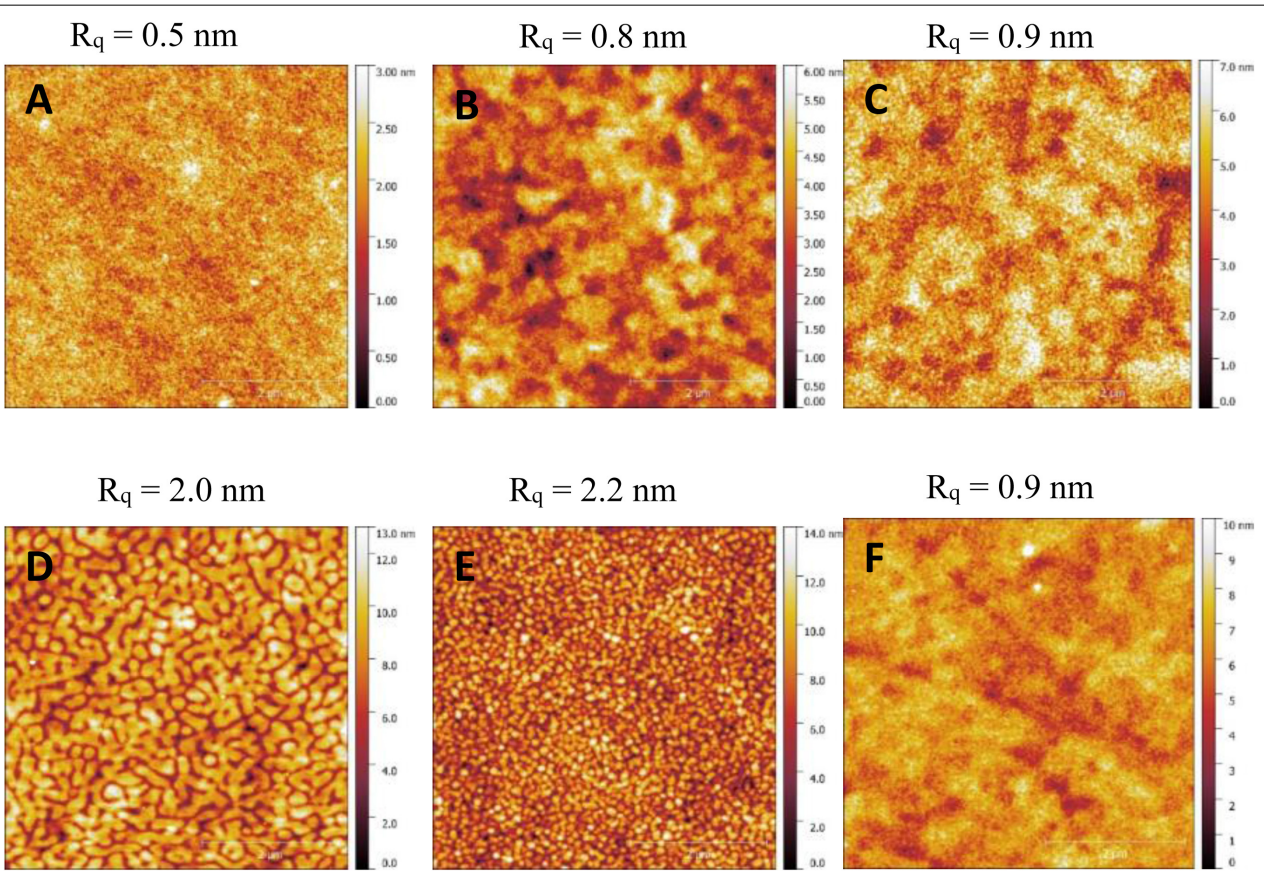

FIGURE 6 | × 5 μM × 5 μM AFM images of **(A)** TQ1A:$PC_{61}BM$, **(B)** TQ1-50A:$PC_{61}BM$, **(C)** TQ1-20A:$PC_{61}BM$, **(D)** TQ1P4:$PC_{61}BM$, **(E)** TQ1-50P4:$PC_{61}BM$, and **(F)** TQ1-20P4:$PC_{61}BM$ films processed from the same solution as device fabrication.

peak of $PC_{61}BM$ in the samples with different polymer:$PC_{61}BM$ ratio (see **Supplementary Figure S8A–C**), agreeing with more phase separation indicated from **Figures 6B,C** compared to **Figure 6A**. Therefore, the improved performance of the amino polymer based OPVs observed with lower content of tertiary amine substituents compared with TQ1A (100% tertiary amine) could be explained by the enhanced phase separation between donor and acceptor by decreasing their interaction. The interaction between pyridine units and fullerenes is likely decreased further, as the conjugate acid of pyridine possesses lower pK_a values (∼5.5) than that of tertiary amines (∼10).

The film containing $PC_{61}BM$ blends of TQ1P4 (**Figure 6D**) or TQ1-50P4 (**Figure 6E**) shows greater phase separated morphology compared to TQ1A:$PC_{61}BM$ film, which could explain the improved photovoltaic performance upon the alteration of donor material from tertiary amine functionalized polymer to TQ1P4 and its analogs in the devices. The TQ1-20P4:$PC_{61}BM$ film exhibits smoother surface compared to other films containing pyridine polymers, resulting from different processing solvent. However, the R_q of it is comparable with TQ1-20A:$PC_{61}BM$ film, indicating similar degree of phase seperation on the surface. Further evidence of the phase separation between TQ1-20P4 and $PC_{61}BM$ was revealed from the DSC result, which clearly shows melting behavior of $PC_{61}BM$ in the blend with D:A ratio of 1:2.5 (**Supplementary Figure S8e**). Therefore, the high degree of miscibility between polar group functionalized polymer and fullerene derivative has to be overcome to achieve sufficient phase separation for OPV operation.

CONCLUSION

Two series of p-type conjugated polymers were successfully synthesized incorporating tertiary amine and pyridine pendant groups, aiming at water and alcohol soluble materials. TQ1A, TQ1-50A, TQ1P4 and TQ1-50P4 showed outstanding switchable solubility in water/ethanol, indicating the potential of processing photoactive materials in an environmentally friendly way. Donor polymers with too high tertiary amine-group content only achieved ∼0.1% PCE, which could be improved to ∼0.8% PCE by decreasing the amino-group content and using a passivating layer of TPD to protect the anode interface. We find that high tertiary amine content increases the miscibility of the donor-acceptor, preventing sufficient phase-separation to occur during drying of the active layer. Solar cells fabricated from TQ1P4:$PC_{61}BM$ achieved a higher PCE of 0.57%, which was further increased to 1.33% for TQ1-50P4. OPVs based on lower content of functionalized group substituted polymers TQ1-20A and TQ1-20P4 offered highest efficiencies of 1.06 and 1.75%, respectively. However, their insolubility in acidic ethanol or water makes them unsuitable for green solvent processed OPVs. Finally, we conclude that by carefully tuning the ratio between polar substituents and hydrophobic alkyl groups is a promising strategy to achieve water/alcohol soluble p-type conjugated polymers as well as decent photovoltaic performance.

DATA AVAILABILITY STATEMENT

All datasets presented in this study are included in the article/**Supplementary Material**.

AUTHOR CONTRIBUTIONS

XP contributed to material synthesis and characterization, part of the device fabrication and characterization, and manuscript writing. AS contributed to the device structure designing and part of the device fabrication. RK contributed to the designing of polymer structure. DG and SE contributed to the electrochemistry experiment. YY and GA contributed to the UPS experiment and results analysis. DL contributed to the manuscript structure suggestion and research funding. MA provided scholarships and contributed to the designing of polymers. All authors have contributed to the modification and correction of the manuscript draft.

FUNDING

This research was supported by the Australian Research Council's Discovery Projects funding scheme (Projects DP170102467 and DP160102356).

ACKNOWLEDGMENTS

The authors thank the Flinders University for financial support. This research was supported by the Australian Research Council's Discovery Projects funding scheme (Projects DP170102467 and DP160102356). The facilities at Flinders University are supported by the Australian Nano Fabrication Facility (ANFF) and the Flinders Microscopy and Microanalysis (FMMA), which are gratefully acknowledged. Special thanks to Qian Li from the Key Laboratory of High Performance Polymer Materials and Technology of Ministry of Education, Nanjing University for the great help with GPC measurements.

SUPPLEMENTARY MATERIAL

The Supplementary Material for this article can be found online at: https://www.frontiersin.org/articles/10.3389/fmats.2020.00281/full#supplementary-material

REFERENCES

Almyahi, F., Andersen, T. R., Cooling, N., Holmes, N. P., Fahy, A., Barr, M. G., et al. (2018). Optimization, characterization and upscaling of aqueous solar nanoparticle inks for organic photovoltaics using low-cost donor:acceptor blend. *Org. Electron.* 52, 71–78. doi: 10.1016/j.orgel.2017.10.008

Angmo, D., Larsen-Olsen, T. T., Jørgensen, M., Søndergaard, R. R., and Krebs, F. C. (2013). Roll-to-Roll inkjet printing and photonic sintering of electrodes

for ITO free polymer solar cell modules and facile product integration. *Adv. Energy Mater.* 3, 172–175. doi: 10.1002/aenm.201200520

Bernardo, G., Deb, N., King, S. M., and Bucknall, D. G. (2016). Phase behavior of blends of PCBM with amorphous polymers with different aromaticity. *J. Polym. Sci. Part B Polym. Phys.* 54, 994–1001. doi: 10.1002/polb.24002

Cai, W., Zhong, C., Duan, C., Hu, Z., Dong, S., Cao, D., et al. (2015). The influence of amino group on PCDTBT-based and P3HT-based polymer solar cells: hole trapping processes. *Appl. Phys. Lett.* 106:233302. doi: 10.1063/1.4922467

Colberts, F. J. M., Wienk, M. M., and Janssen, R. A. J. (2017). Aqueous nanoparticle polymer solar cells: effects of surfactant concentration and processing on device performance. *ACS Appl. Mater. Interfaces* 9, 13380–13389. doi: 10.1021/acsami.7b00557

Dang, D., Chen, J., Zhou, P., Duan, L., Bao, X., Yang, R., et al. (2016). Tuning the fused aromatic rings to enhance photovoltaic performance in wide band-gap polymer solar cells. *Polymer* 104, 130–137. doi: 10.1016/j.polymer.2016.10.011

D'Olieslaeger, L., Pirotte, G., Cardinaletti, I., D'Haen, J., Manca, J., Vanderzande, D., et al. (2017). Eco-friendly fabrication of PBDTTPD:PC71BM solar cells reaching a PCE of 3.8% using water-based nanoparticle dispersions. *Org. Electron.* 42, 42–46. doi: 10.1016/j.orgel.2016.12.018

Duan, C., Cai, W., Hsu, B. B. Y., Zhong, C., Zhang, K., Liu, C., et al. (2013). Toward green solvent processable photovoltaic materials for polymer solar cells: the role of highly polar pendant groups in charge carrier transport and photovoltaic behavior. *Energy Environ. Sci.* 6, 3022–3034.

Fan, B., Ying, L., Wang, Z., He, B., Jiang, X.-F., Huang, F., et al. (2017). Optimisation of processing solvent and molecular weight for the production of green-solvent-processed all-polymer solar cells with a power conversion efficiency over 9%. *Energy Environ. Sci.* 10, 1243–1251. doi: 10.1039/c7ee00619e

Fan, Q., Ma, R., Liu, T., Su, W., Peng, W., Zhang, M., et al. (2020). 10.*13*% efficiency all-polymer solar cells enabled by improving the optical absorption of polymer acceptors. *Solar RRL* 4:2000142. doi: 10.1002/solr.202000142

Gärtner, S., Christmann, M., Sankaran, S., Röhm, H., Prinz, E.-M., Penth, F., et al. (2014). Eco-friendly fabrication of 4% efficient organic solar cells from surfactant-free P3HT:ICBA nanoparticle dispersions. *Adv. Mater.* 26, 6653–6657. doi: 10.1002/adma.201402360

Gedefaw, D., Prosa, M., Bolognesi, M., Seri, M., and Andersson, M. R. (2017a). Recent development of quinoxaline based polymers/small molecules for organic photovoltaics. *Adv. Energy Mater.* 7:1700575. doi: 10.1002/aenm.201700575

Gedefaw, D., Sharma, A., Pan, X., Bjuggren, J. M., Kroon, R., Gregoriou, V. G., et al. (2017b). Optimization of the power conversion efficiency in high bandgap pyridopyridinedithiophene-based conjugated polymers for organic photovoltaics by the random terpolymer approach. *Eur. Polym. J.* 91, 92–99. doi: 10.1016/j.eurpolymj.2017.03.044

Geoffrey, P., Laurie, P., Eleni, P., Gilles, P., Cyril, B., Georges, H., et al. (2018). Aqueous PCDTBT:PC71BM photovoltaic inks made by nanoprecipitation. *Macromol. Rapid Commun.* 39:1700504. doi: 10.1002/marc.201700504

George, Z., Xia, Y., Sharma, A., Lindqvist, C., Andersson, G., Inganäs, O., et al. (2016). Two-in-one: cathode modification and improved solar cell blend stability through addition of modified fullerenes. *J. Mater. Chem. A* 4, 2663–2669. doi: 10.1039/c5ta06420a

Ghosh, H. N., Pal, H., Sapre, A. V., and Mittal, J. P. (1993). Charge recombination reactions in photoexcited fullerene C60-amine complexes studied by picosecond pump probe spectroscopy. *J. Am. Chem. Soc.* 115, 11722–11727. doi: 10.1021/ja00078a010

He, Z., Wu, H., and Cao, Y. (2014). Recent advances in polymer solar cells: realization of high device performance by incorporating water/alcohol-soluble conjugated polymers as electrode buffer layer. *Adv. Mater.* 26, 1006–1024. doi: 10.1002/adma.201303391

Hellström, S., Henriksson, P., Kroon, R., Wang, E., and Andersson, M. R. (2011). Blue-to-transmissive electrochromic switching of solution processable donor–acceptor polymers. *Org. Electron.* 12, 1406–1413. doi: 10.1016/j.orgel.2011.05.008

Hellström, S., Zhang, F., Inganäs, O., and Andersson, M. R. (2009). Structure-property relationships of small bandgap conjugated polymers for solar cells. *Dalton Trans.* 45, 10032–10039.

Holmes, N. P., Marks, M., Kumar, P., Kroon, R., Barr, M. G., Nicolaidis, N., et al. (2016). Nano-pathways: bridging the divide between water-processable nanoparticulate and bulk heterojunction organic photovoltaics. *Nano Energy* 19, 495–510. doi: 10.1016/j.nanoen.2015.11.021

Hu, Z., Zhang, K., Huang, F., and Cao, Y. (2015). Water/alcohol soluble conjugated polymers for the interface engineering of highly efficient polymer light-emitting diodes and polymer solar cells. *Chem. Commun.* 51, 5572–5585. doi: 10.1039/c4cc09433f

Huang, F., Wu, H., and Cao, Y. (2010). Water/alcohol soluble conjugated polymers as highly efficient electron transporting/injection layer in optoelectronic devices. *Chem. Soc. Rev.* 39, 2500–2521.

Ishii, H., Sugiyama, K., Ito, E., and Seki, K. (1999). Energy level alignment and interfacial electronic structures at organic/metal and organic/organic interfaces. *Adv. Mater.* 11, 605–625. doi: 10.1002/(sici)1521-4095(199906)11:8<605::aid-adma605>3.0.co;2-q

Kim, Y., Choi, J., Lee, C., Kim, Y., Kim, C., Nguyen, T. L., et al. (2018). Aqueous soluble fullerene acceptors for efficient eco-friendly polymer solar cells processed from benign ethanol/water mixtures. *Chem. Mater.* 30, 5663–5672. doi: 10.1021/acs.chemmater.8b02086

Krebs, F. C., Gevorgyan, S. A., and Alstrup, J. (2009). A roll-to-roll process to flexible polymer solar cells: model studies, manufacture and operational stability studies. *J. Mater. Chem.* 19:5442. doi: 10.1039/b823001c

Krebs, F. C., Tromholt, T., and Jorgensen, M. (2010). Upscaling of polymer solar cell fabrication using full roll-to-roll processing. *Nanoscale* 2, 873–886.

Kröger, M., Hamwi, S., Meyer, J., Riedl, T., Kowalsky, W., and Kahn, A. (2009). Role of the deep-lying electronic states of MoO3 in the enhancement of hole-injection in organic thin films. *Appl. Phys. Lett.* 95:123301. doi: 10.1063/1.3231928

Kroon, R., Gehlhaar, R., Steckler, T. T., Henriksson, P., Müller, C., Bergqvist, J., et al. (2012). New quinoxaline and pyridopyrazine-based polymers for solution-processable photovoltaics. *Sol. Energy Mater. Sol. Cells* 105, 280–286. doi: 10.1016/j.solmat.2012.06.029

Lee, C., Lee, H. R., Choi, J., Kim, Y., Nguyen, T. L., Lee, W., et al. (2018). Efficient and air-stable aqueous-processed organic solar cells and transistors: impact of water addition on processability and thin-film morphologies of electroactive materials. *Adv. Energy Mater.* 8, 1802674. doi: 10.1002/aenm.201802674

Lee, S., Kim, Y., Wu, Z., Lee, C., Oh, S. J., Luan, N. T., et al. (2019). Aqueous-soluble naphthalene diimide-based polymer acceptors for efficient and air-stable all-polymer solar cells. *ACS Appl. Mater. Interfaces* 11, 45038–45047. doi: 10.1021/acsami.9b13812

Lee, J., Seo, Y. H., Kwon, S. N., Kim, D. H., Jang, S., Jung, H., et al. (2019). Slot-die and roll-to-roll processed single junction organic photovoltaic cells with the highest efficiency. *Adv. Energy Mater.* 9:1901805. doi: 10.1002/aenm.201901805

Li, S., Lei, M., Lv, M., Watkins, S. E., Tan, Z. A., Zhu, J., et al. (2013). [6,6]-Phenyl-C61-butyric acid dimethylamino ester as a cathode buffer layer for high-performance polymer solar cells. *Adv. Energy Mater.* 3, 1569–1574. doi: 10.1002/aenm.201300425

Li, X., Huang, G., Zheng, N., Li, Y., Kang, X., Qiao, S., et al. (2019). High-efficiency polymer solar cells over 13.9% with a high voc beyond 1.0 V by synergistic effect of fluorine and sulfur. *Solar RRL* 3:1900005. doi: 10.1002/solr.201900005

Li, Z., Ying, L., Zhu, P., Zhong, W., Li, N., Liu, F., et al. (2019). A generic green solvent concept boosting the power conversion efficiency of all-polymer solar cells to 11%. *Energy Environ. Sci.* 12, 157–163. doi: 10.1039/c8ee02863j

Li, Z., Xie, R., Zhong, W., Fan, B., Ali, J., Ying, L., et al. (2018). High-performance green solvent processed ternary blended all-polymer solar cells enabled by complementary absorption and improved morphology. *Solar RRL* 2:1800196. doi: 10.1002/solr.201800196

Liu, Q., Jiang, Y., Jin, K., Qin, J., Xu, J., Li, W., et al. (2020). 18% efficiency organic solar cells. *Sci. Bull.* 65, 272–275.

Lu, K., Yuan, J., Peng, J., Huang, X., Cui, L., Jiang, Z., et al. (2013). New solution-processable small molecules as hole-transporting layer in efficient polymer solar cells. *J. Mater. Chem. A* 1:14253. doi: 10.1039/c3ta12935g

Lv, M., Lei, M., Zhu, J., Hirai, T., and Chen, X. (2014). [6,6]-phenyl-C(6)(1)-butyric acid 2-((2-(dimethylamino)ethyl)(methyl)amino)-ethyl ester as an acceptor and cathode interfacial material in polymer solar cells. *ACS Appl. Mater. Interfaces* 6, 5844–5851. doi: 10.1021/am5007047

Ma, D., Lv, M., Lei, M., Zhu, J., Wang, H., and Chen, X. (2014). Self-organization of amine-based cathode interfacial materials in inverted polymer solar cells. *ACS Nano* 8, 1601–1608. doi: 10.1021/nn4059067

Mei, J., and Bao, Z. (2013). Side chain engineering in solution-processable conjugated polymers. *Chem. Mater.* 26, 604–615. doi: 10.1021/cm4020805

Meyer, J., Hamwi, S., Kroger, M., Kowalsky, W., Riedl, T., and Kahn, A. (2012). Transition metal oxides for organic electronics: energetics, device physics and applications. *Adv. Mater.* 24, 5408–5427. doi: 10.1002/adma.201201630

Mwaura, J. K., Pinto, M. R., Witker, D., Ananthakrishnan, N., Schanze, K. S., and Reynolds, J. R. (2005). Photovoltaic cells based on sequentially adsorbed multilayers of conjugated poly (p-phenylene ethynylene) s and a water-soluble fullerene derivative. *Langmuir* 21, 10119–10126. doi: 10.1021/la050599m

Nguyen, T. L., Lee, C., Kim, H., Kim, Y., Lee, W., Oh, J. H., et al. (2017). Ethanol-processable, highly crystalline conjugated polymers for eco-friendly fabrication of organic transistors and solar cells. *Macromolecules* 50, 4415–4424. doi: 10.1021/acs.macromol.7b00452

Pan, X., Sharma, A., Gedefaw, D., Kroon, R., Diaz de Zerio, A., Holmes, N. P., et al. (2018). Environmentally friendly preparation of nanoparticles for organic photovoltaics. *Org. Electron.* 59, 432–440. doi: 10.1016/j.orgel.2018.05.040

Park, K.-Y., Lee, J.-S., Namkung, H.-S., Koo, M.-S., Cho, S.-J., Yoon, B.-W., et al. (2015). Enhanced performance in bulk heterojunction polymer solar cell using water soluble conjugated polymer. *J. Nanosci. Nanotechnol.* 15, 1683–1686. doi: 10.1166/jnn.2015.9305

Schwarz, K. N., Farley, S. B., Smith, T. A., and Ghiggino, K. P. (2015). Charge generation and morphology in P3HT:PCBM nanoparticles prepared by mini-emulsion and reprecipitation methods. *Nanoscale* 7, 19899–19904. doi: 10.1039/c5nr06244f

Sharma, A., Kroon, R., Lewis, D. A., Andersson, G. G., and Andersson, M. R. (2017). Poly(4-vinylpyridine): a new interface layer for organic solar cells. *ACS Appl. Mater. Interfaces* 9, 10929–10936. doi: 10.1021/acsami.6b12687

Søndergaard, R., Helgesen, M., Jørgensen, M., and Krebs, F. C. (2011). Fabrication of polymer solar cells using aqueous processing for all layers including the metal back electrode. *Adv. Energy Mater.* 1, 68–71. doi: 10.1002/aenm.201000007

Søndergaard, R., Hösel, M., Angmo, D., Larsen-Olsen, T. T., and Krebs, F. C. (2012). Roll-to-roll fabrication of polymer solar cells. *Mater. Today* 15, 36–49. doi: 10.1016/s1369-7021(12)70019-6

Subbiah, J., Kim, D. Y., Hartel, M., and So, F. (2010). MoO3/poly(9,9-dioctylfluorene-co-N-[4-(3-methylpropyl)]-diphenylamine) double-interlayer effect on polymer solar cells. *Appl. Phys. Lett.* 96:063303. doi: 10.1063/1.3310013

Sun, Y., Seo, J. H., Takacs, C. J., Seifter, J., and Heeger, A. J. (2011). Inverted polymer solar cells integrated with a low-temperature-annealed sol-gel-derived ZnO film as an electron transport layer. *Adv. Mater.* 23, 1679–1683. doi: 10.1002/adma.201004301

van Reenen, S., Kouijzer, S., Janssen, R. A. J., Wienk, M. M., and Kemerink, M. (2014). Origin of work function modification by ionic and amine-based interface layers. *Adv. Mater. Interfaces* 1:1400189. doi: 10.1002/admi.201400189

Venkatesan, S., Chen, Q., Ngo, E. C., Adhikari, N., Nelson, K., Dubey, A., et al. (2014). Polymer solar cells processed using anisole as a relatively nontoxic solvent. *Energy Technol.* 2, 269–274. doi: 10.1002/ente.201300174

Wang, E., Hou, L., Wang, Z., Hellstrom, S., Zhang, F., Inganas, O., et al. (2010). An easily synthesized blue polymer for high-performance polymer solar cells. *Adv. Mater.* 22, 5240–5244. doi: 10.1002/adma.201002225

Wang, Y., Fan, Q., Guo, X., Li, W., Guo, B., Su, W., et al. (2017). High-performance nonfullerene polymer solar cells based on a fluorinated wide bandgap copolymer with a high open-circuit voltage of 1.*04* V. *J. Mater. Chem. A* 5, 22180–22185. doi: 10.1039/c7ta07785h

Woo, H. Y., Liu, B., Kohler, B., Korystov, D., Mikhailovsky, A., and Bazan, G. C. (2005). Solvent effects on the two-photon absorption of distyrylbenzene chromophores. *J. Am. Chem. Soc.* 127, 14721–14729. doi: 10.1021/ja052906g

Wu, Z., Sun, C., Dong, S., Jiang, X. F., Wu, S., Wu, H., et al. (2016). n-Type water/alcohol-soluble naphthalene diimide-based conjugated polymers for high-performance polymer solar cells. *J. Am. Chem. Soc.* 138, 2004–2013. doi: 10.1021/jacs.5b12664

Xie, C., Tang, X., Berlinghof, M., Langner, S., Chen, S., Spath, A., et al. (2018). Robot-based high-throughput engineering of alcoholic polymer: fullerene nanoparticle inks for an eco-friendly processing of organic solar cells. *ACS Appl. Mater. Interfaces* 10, 23225–23234. doi: 10.1021/acsami.8b03621

Xing, X., Zeng, Q., Vagin, M., Fahlman, M., and Zhang, F. (2018). Fast switching polymeric electrochromics with facile processed water dispersed nanoparticles. *Nano Energy* 47, 123–129. doi: 10.1016/j.nanoen.2018.02.050

Xu, B., Zheng, Z., Zhao, K., and Hou, J. (2016). A bifunctional interlayer material for modifying both the anode and cathode in highly efficient polymer solar cells. *Adv. Mater.* 28, 434–439. doi: 10.1002/adma.201502989

Xu, X., Li, Z., Wang, Z., Li, K., Feng, K., and Peng, Q. (2016). 10.*20*% Efficiency polymer solar cells via employing bilaterally hole-cascade diazaphenanthrobisthiadiazole polymer donors and electron-cascade indene-C70 bisadduct acceptor. *Nano Energy* 25, 170–183. doi: 10.1016/j.nanoen.2016.04.048

Xu, X., Yu, T., Bi, Z., Ma, W., Li, Y., and Peng, Q. (2017). Realizing over 13% efficiency in green-solvent-processed nonfullerene organic solar cells enabled by 1,3,4-Thiadiazole-based wide-bandgap copolymers. *Adv. Mater.* 30:1703973. doi: 10.1002/adma.201703973

Xue, R., Zhang, J., Li, Y., and Li, Y. (2018). Organic solar cell materials toward commercialization. *Small* 14:e1801793.

Yang, J., Garcia, A., and Nguyen, T.-Q. (2007). Organic solar cells from water-soluble poly(thiophene)/fullerene heterojunction. *Appl. Phys. Lett.* 90:103514. doi: 10.1063/1.2711707

Yu, Y.-Y., Tsai, T.-W., Yang, C.-C., and Chen, C.-P. (2017). Highly efficient non-fullerene organic photovoltaics processed from o-Xylene without using additives. *J. Mater. Chem. C* 121, 21969–21974. doi: 10.1021/acs.jpcc.7b07867

Zhang, S., Ye, L., Zhang, H., and Hou, J. (2016). Green-solvent-processable organic solar cells. *Mater. Today* 19, 533–543. doi: 10.1016/j.mattod.2016.02.019

Zhang, W., Song, C., Li, Y., Liu, X., Wang, X., Sun, X., et al. (2017). Highly efficient polymer solar cells with PTB7-based narrow band-gap conjugated polyelectrolytes as cathode interlayers: device performance dependence on the ionic pendants. *Org. Electron.* 47, 94–101. doi: 10.1016/j.orgel.2017.04.026

Conflict of Interest: The authors declare that the research was conducted in the absence of any commercial or financial relationships that could be construed as a potential conflict of interest.